Combined High-Energy Synchrotron X-Ray Diffraction and Computed Tomography to Characterize Constitutive Behavior of Silica Sand

Mehmet B. Cil[1], Khalid Alshibli[2], Peter Kenesei[3], and Ulrich Lienert[4]

Abstract: The deformation behavior of silica sand particles under one-dimensional (1D) loading compression was investigated using nondestructive 3D synchrotron micro-computed tomography (SMT) and three dimensional x-ray diffraction (3DXRD). High-resolution SMT images were used to monitor particle-to-particle interactions, and the onset and propagation of fracture mechanism in a column composed of three silica sand particles. Particle-averaged lattice strain tensors within individual sand particles were measured using the 3DXRD technique and were then used to calculate the stress tensor components via the general elastic stress-strain relationship. The normal stress component in the axial direction (σ_{zz}) exhibited a nearly linear increasing trend in all sand particles. Shear stress components were in general small relative to the normal stress components and displayed no systematic trend. Knowing lattice strains, stresses, and particle kinematic behavior, one can formulate and develop a micromechanics-based constitutive model to fully characterize strength properties and deformation characteristics of granular materials.

Keywords: Granular materials, lattice strain, stress, 3D x-ray diffraction

---

[1] Graduate student, Department of Civil and Environmental Engineering, University of Tennessee, Knoxville, TN 37996, USA [email: mcil@utk.edu]

[2] Professor, Department of Civil and Environmental Engineering, University of Tennessee, Knoxville, TN 37996, USA [email: Alshibli@utk.edu]

[3] Research Scientist, Argonne National Laboratory, Argonne, Illinois, USA [email: kenesei@aps.anl.gov]

[4] Research Scientist, Deutsches Elektronen-Synchrotron, DESY Photon Science, Hamburg, Germany [email: ulrich.lienert@desy.de]

1. Introduction

The common use of granular materials in various engineering and science applications promotes the need to develop advanced constitutive models to better predict the macroscopic response of discrete systems under various loading conditions. Many constitutive models were developed based on the elasto-plastic theory and continuum mechanics in which the discrete nature of the particulate system on the microscale-level was not taken into account [e.g., 1, 2, 3]. The stress-strain behavior of granular materials is governed by complex micromechanical processes including particle translation, rotation, and fracture, which need to be considered while developing a comprehensive mathematical model. The first prerequisite of developing a micromechanics-based constitutive model is to measure micro-scale properties of the material. Discrete element method (DEM), introduced by Cundall and Strack [4], provided a framework to investigate the independent interaction of individual particles and permitted acquiring particle-level measurements including contact forces, which are impossible to obtain using conventional experimental techniques [5]. DEM's applicability for modeling engineering applications is limited, however, by its inability to represent real particle morphology and the expensive computational time necessary for large specimens.

The limitations of numerical and theoretical approaches motivated many researchers to explore alternative options, and promising new powerful experimental techniques such as x-ray computed tomography (CT) have emerged as alternative solutions to gain insight into micromechanical processes that occur during the deformation of granular media [6]. X-ray CT and its advanced version, synchrotron micro-computed tomography (SMT), are non-invasive 3D imaging techniques that have been used in a wide range of applications including geomaterial studies. SMT can yield a high-resolution 3D image of particulate system which allows in situ

monitoring of the deformation mechanisms and particle kinematics [e.g., 7, 8]. However, SMT does not provide measurements of inter-particle forces or strains within the particle itself.

Three dimensional x-ray diffraction (3DXRD) is a revolutionary non-destructive experimental technique for characterizing the structure of polycrystalline materials. It allows robust determination of the crystallographic orientation, position, and shape of individual grains embedded in the bulk of specimen with a high resolution. Moreover, 3DXRD provides a unique opportunity to investigate the deformation behavior of microstructural elements under macroscopic loading [9-12]; the kinetics of grains during recrystallization [13, 14]; the nucleation and growth processes in solid-state phase transformation [15]; and the rotation of grains under deformation [16]. Moreover, many models associated with the evolution and interaction of microstructures can be validated and improved with the help of measurements acquired through the 3DXRD method [17]. Poulsen [18] presented the basic principles, instrumentation, and groundbreaking applications of 3DXRD. The majority of 3DXRD applications were utilized in studies related to metals. On the granular materials side, Hall et al. [19] presented preliminary results of 3DXRD scanning on Ottawa sand specimens that were subjected to one-dimensional (1D) loading. However, their analysis did not include extracting lattice strain tensor measurements from the data.

In this study, SMT and 3DXRD methods are combined to gain insight into the deformation characteristics of sand particles under 1D loading condition. The main objective of this paper is to describe the experimental methodologies of both techniques and to determine grain-averaged stress-strain tensors of individual silica sand particles.

2. Experimental Techniques

2.1. *SMT Scanning Technique*

SMT is a non-destructive 3D imaging technique that has been extensively used in various fields such as biological and geological specimen studies in the last few decades. It can produce 3D high-resolution images through mapping the attenuation data as x-ray beam travels through the specimen. SMT has become available with the development of third-generation synchrotron facilities, which have provided a unique opportunity to obtain collimated and tunable high photon flux radiation. A high energy monochromatic x-ray beam generated from a synchrotron source passes through a specimen positioned on a rotation stage between the incoming x-ray beam and scintillator (Figure 1). Some of the photons are absorbed by the specimen, which primarily depends on the electron density distribution within the specimen and the energy of the x-rays.

The linear attenuation coefficient is strongly dependent on the atomic number of the elements within the sample. The transmitted x-rays are converted to visible light through a scintillator and recorded using a high-resolution detector. To obtain a 3D volumetric image, a series of projections must be acquired while rotating the sample typically from 0° to 180° with 0.1° to 1° increments. During this process, flat field images which map the incoming x-ray beam profile are also collected for the reconstruction process to normalize the measured transmission maps. Multiple scans at consecutive vertical specimen positions are performed if the height is longer than the beam height. Data processing can be summarized as dark field correction, normalization, determination of the rotation axis and reconstruction of the 3D volumetric data, which results in a stack of 2D slices [20, 21]. These slices contain the spatial distribution map of the x-ray attenuation of the specimen. In this study, the raw scan data is processed via

user-written scripts in an Interactive Data Language (IDL) program, which uses the GridRec algorithm written in C to reconstruct 3D images.

2.2. *3DXRD Technique*

3DXRD was developed by a research group from the Risø National Laboratory (Denmark) at the European Synchrotron Radiation Facility (ESRF, France), which commissioned the first dedicated instrument in 1999. The basic working mechanism of the 3DXRD method is tracking diffracted hard x-rays using a transmission-based data collection system (Figure 2). The x-ray radiation provided by the synchrotron storage ring passes through a series of specially fabricated optics, which produce a monochromatic high energy x-ray beam while maintaining the high brilliance. The main advantage of hard x-rays over low energy x-rays is the high penetration power, which makes it suitable for studying the bulk specimen behavior of various polycrystalline materials. The desired beam size in horizontal and vertical directions is determined based on the average grain size of the material and specimen thickness and is adjusted using a group of slits. Then, the high-energy x-ray beam impinges on the specimen, which is positioned on high precision rotational and translational stages between incoming beam and data acquisition system. Some crystallites of the illuminated specimen satisfy the Bragg condition and give rise to diffracted beams, which are transmitted through the specimen and recorded by a 2D area detector. Due to the high energy x-ray with short wavelength, the diffraction angles 2θ are smaller than at low energies, therefore several diffraction orders can be acquired on a single area detector. To probe the whole specimen, the specimen must be rotated perpendicular to the beam direction with angular rotation increments ($\Delta\omega$). If the specimen dimensions are larger than the beam size, multiple scans are acquired at different positions.

The detector configuration is determined based on the objective of the experiment (e.g., 3D mapping of grains or investigating microstructural kinetics during typical processes). Since the objective of this study is to measure the grain deformation under compressive loading, a far-field detector configuration was adopted to probe the orientation and deformation in the grain lattice.

3. EXPERIMENTS

3.1. *Testing apparatus*

The sand used in the experiments is a natural uniform silica sand known as ASTM 20-30 Ottawa sand with particle sizes between 0.595 mm (Sieve No. 30) and 0.841 mm (Sieve No. 20). The experiments were conducted using a specially designed test cell that consists of a loading system, a specimen mold, load cells, and a data acquisition system (Figure 3). The compressive load was applied using a high precision computerized stepper motor that can apply a displacement rate as small as 0.0125 mm/min. The specimen mold consists of an acrylic cylinder with a diameter of 15 mm and a 1 mm hole at the center. Two load cells were attached to the top and bottom of the specimen to measure load reduction due to friction between particles and the mold. This setup is supported by a hollow cylindrical acrylic chamber bolted to the top and bottom cell plates. Only three sand particles were placed inside the 1 mm hole as a column to eliminate plugging of particles during compression. The sand column was scanned before the axial load was applied; it was then loaded until the desired compressive load was reached, and the scan was performed while the stepper motor position was held in position. This procedure was repeated for consecutive load levels and scans.

3.2. *SMT scans*

The SMT scans were conducted at the Advanced Photon Source (APS), GeoSoilEnviroCARS (GSECARS) Sector 13 of the Argonne National Laboratory (ANL), Illinois, USA. The x-ray beam was monochromatized using a Si (111) double crystal monochromator that preserves the high flux of the x-rays. To obtain high-resolution images in a relatively small specimen size (~1 mm diameter × ~2.4 mm height), the attenuated x-rays were acquired by an imaging system consisting of a single crystal scintillator, a 5x microscope objective and a 1392 × 1040 pixel resolution CoolSnap HQ^2 CCD camera from Roper Scientific, which provided an image resolution of 4.95 μm/pixel. The scans were carried out at an x-ray energy of 23 keV. X-ray images were collected at 0.25° increments by rotating the specimen over 180° and applying 1 second exposure time, which produced 720 frames per scan. 3D SMT images were acquired at multiple load levels for three compression experiments.

3.3. *3DXRD scans*

The 3DXRD experiments were performed at the 1-ID beamline of the APS. The test cell was mounted on the high precision specimen stages, which provide translation in x, y, and z direction along with the rotation around the z-axis. The sand particles were illuminated by a high-energy x-ray beam with a size of 1.0 mm × 0.8 mm and an energy of 80.725 keV that corresponds to a wavelength of 0.15358 Å. 3DXRD data were acquired by rotating the specimen at a constant angular velocity about an axis perpendicular to the beam direction. The beam was centered to completely illuminate the 1 mm diameter that contains the particle column, and rotation scans were collected at three successive vertical levels. Diffraction data were acquired by an area detector that was positioned at a horizontal distance of 1593 mm (*L* in Figure 2) from

the specimen. An intensity distribution image of the diffracted spots (called the ω-slice) was recorded at each rotation interval of $\Delta\omega$. The raw diffraction data consist of 180 stacked images recorded while the specimen was rotated in ω from -90° to 90° with $\Delta\omega = 1°$ integration intervals at each loading step for each particle. Three 1D compression experiments were conducted at displacement rates of 0.0125 mm/min, 0.05 mm/min, and 0.2 mm/min. Multiple 3DXRD scans were collected at various load levels.

4. Results

4.1. *SMT imaging*

An example load-displacement relationship of 1D compression experiments conducted during SMT scans is depicted in Figure 4a, which shows that the compressive load level increases gradually as compression progresses. Compressive forces, displacement, stress, and strain are taken as positive throughout this paper according to the sign convention in the field of geotechnical engineering. Some small load drops due to particle movement are observed before the major fracture of one of the particles which leads to a significant load drop. A scatter curve emerges after the initial fracture, which results from the continuing fracture of broken fragments of the fractured particle. The axial cross sectional images of the specimen acquired at consecutive load steps are shown in Figure 4b, which clearly demonstrates the compressive behavior of individual sand particles under 1D compression. Initially, particles slightly rearrange via rotation and/or translation, and reach a stable configuration in which lateral support is provided by the mold walls. Then, the column of particles resists the increasing compressive load until fracture occurs in the form of catastrophic splitting. Both fractured and intact particles continue to fracture as the compression progresses.

4.2. *The advantages of combining SMT and 3DXRD data*

SMT provides valuable 3D images of sand particles that cannot be obtained through the 3DXRD method. SMT images enable in situ monitoring of the fracture mechanism and particle kinematic behavior. Examining the 3D images of the specimen demonstrated that particles experience translation and/or rotation before fracture due to the interaction of discrete particles at the contact points. The positional change of sand particles resulted in the translation of diffraction spots in 3DXRD scans, which is not observed in the majority of the 3DXRD applications performed on metals. Therefore, the motion of sand particles due to axial loading has to be considered while evaluating the diffraction data. One of the drawbacks of the 3DXRD method is that it does not allow visualization of the initiation and propagation of fracture. This limitation was eliminated by using complementary SMT that has proven very helpful in the selection of the load steps for the 3DXRD measurements to investigate the evolution of lattice strain before fracture. In addition, compressive displacement can be measured with a high degree of precision by calculating the motion of loading platens or tracking particle positions in SMT images.

4.3. *Measuring Particle Strain*

Since only one or two sand particles were illuminated in all scans until the first particle fracture occurrence in the system, 2D diffraction images are composed of a limited number of separated diffraction spots on the Debye-Scherrer rings, which makes the data evaluation process easy to handle compared to 3DXRD data with overlapped spots. The analysis of the diffraction data was carried out by following a series of steps consisting of peak searching, indexing, and the computation of lattice stress-strain tensor components. First, the DIGIgrain program that was

developed by Kenesei [22] was used to perform several background corrections on the acquired raw diffraction images and to identify the diffraction spots by deploying a 3D peak search. The program provided a list of diffraction peaks along with their properties including position and intensity. Then, g-vectors (diffraction vectors) were computed based on the identified peaks with the Image11 transformation program [23] which also enables to calibrate detector distance and beam center. These g-vectors were assigned to the corresponding grains with the help of the GrainSpotter indexing program [24]. The results are summarized in an output file that includes the indexed grains and their properties (orientation, 3D center of mass position, the list of associated diffraction peaks).

The next step is the determination of the elastic grain deformation that was executed using a Matlab script written by the authors. The lattice-strain was calculated by measuring the changes in the magnitude of g-vectors relative to the unloaded grain condition. The grain averaged strain tensor (ε_i) components were calculated based on the following equation:

$$\varepsilon_i = \frac{g_i - g_i^0}{g_i^0} \tag{1}$$

where g_i^0 and g_i are the length of the g-vectors in the unloaded and loaded cases, respectively. For each load level, the corresponding g-vectors were identified and compared with the initial strain-free condition. Details of the strain calculation process are presented in Alshibli et al. [25].

Since all strain tensor components are obtained from the diffraction analysis, the grain stress (σ_i) could be derived using the general elastic constitutive relationship. The fourth-rank stiffness tensor, which relates strain to stress can be contracted to a six-by-six matrix in the Voigt contraction notation as follows:

$$\sigma_i = c_{ij}\varepsilon_j \qquad i,j = 1 \ldots 6 \tag{2}$$

where c_{ij} is the elastic stiffness tensor in contracted form. The anisotropic elastic structure of the quartz was taken into account while inferring stresses from the grain averaged strain tensors, and the elastic constants of quartz were obtained from Heyliger et al. [26] The stress tensor components in the sample coordinate system were calculated from the measured strain tensor components using Equation 2 and appropriate coordinate system transformations.

The stress-strain relationships of the normal stress components of top particles in Tests 1, 2, and 3 are depicted in Figure 5 which demonstrates that σ_{xx} and σ_{yy} exhibit complex deformation behavior resulting from the combined effects of various micromechanical processes such as the translation and rotation of particles and the effect of boundary conditions. Moreover, σ_{xx} and σ_{yy} components are small relative to σ_{zz} component, reflecting the 1D loading mode. Also, the small Poisson's ratio in silica sand particles should be noted. Since shear strain components are very small compared to normal stress components in all cases, they were not plotted in Figure 5. The majority of the shear stress components are an order of magnitude smaller than the normal stresses and exhibited a nonlinear continuous variation throughout the loading, which is mainly governed by particle shape, contact point orientation, particle movement, and fabric. As depicted in SMT images shown in Figure 4b, particles rearrange during the deformation process and come in contact with the mold and neighbor particles in multiple directions, which produces a highly complex particulate system that is difficult to interpret

Figure 6 shows the normal stress component in the loading direction (σ_{zz}) of all silica sand particles up to the fracture of one of the particles in the sand column. A nearly linear stress-strain relationship is evident in all sand particles under 1D loading as expected. The

variation between components stems from several factors including particle motion, or interactions between particle and boundary conditions. Overall, the results show a very consistent elastic behavior in the direction of loading.

5. Conclusions

The SMT and 3DXRD techniques complement each other to provide insight into the constitutive behavior of silica sand particles that were subjected to 1D compression. The SMT imaging technique enabled in situ visualization of particle kinematic behavior and the evolution of fracture mechanism. The stress-strain relationship of silica sand particles under 1D loading was examined based on 3DXRD scans. The σ_{zz} stress component of all sand particles in the direction of loading varied linearly in agreement with the expectations. On the other hand, normal stress (σ_{xx}, σ_{yy}) and shear stress components are relatively small and exhibited inconsistent and nonlinear trends in the majority of the particles under the influence of various micro-scale processes. Combining SMT and 3DXRD offers excellent particle-level measurements that can be used to develop a micromechanics-based constitutive model of granular materials.

Acknowledgements

This material is based on work supported by the National Science Foundation (NSF) under Grant No. CMMI-1156436. The 3DXRD data were collected using the Beamline 1-ID and SMT scans were collected using Beamline 13 at the Advanced Photon Source (APS), Argonne National Laboratory (ANL), USA. We thank Dr. Mark Rivers of APS for help in performing the SMT scans. We also acknowledge the support of GeoSoilEnviroCARS (Sector 13), which is supported by the National Science Foundation-Earth Sciences (EAR-1128799), and the

Department of Energy (DOE), Geosciences (DE-FG02-94ER14466). Use of the APS, an Office of Science User Facility operated for the DOE Office of Science by Argonne National Laboratory, was supported by DOE under Contract No. DE-AC02-06CH11357

References

[1] R.I. Borja, J.E. Andrade, Critical state plasticity. Part VI: Meso-scale finite element simulation of strain localization in discrete granular materials, Computer Methods in Applied Mechanics and Engineering, 195 (2006) 5115-5140.
[2] M.T. Manzari, Y.F. Dafalias, A critical state two-surface plasticity model for sands, Geotechnique, 47 (1997) 255-272.
[3] A.R. Russell, N. Khalili, A unified bounding surface plasticity model for unsaturated soils, International Journal for Numerical and Analytical Methods in Geomechanics, 30 (2006) 181-212.
[4] P. Cundall, O. Strack, A Discrete Numerical model for Granular Assemblies, Geotechnique, 29 (1979) 47-65.
[5] C. O'Sullivan, L. Cui, Micromechanics of granular material response during load reversals: Combined DEM and experimental study, Powder Technol, 193 (2009) 289-302.
[6] T. Matsushima, J. Katagiri, K. Uesugi, T. Nakano, A. Tsuchiyama, Micro X-Ray Ct At Spring-8 For Granular Mechanics, in: H. Ling, L. Callisto, D. Leshchinsky, J. Koseki (Eds.) Soil Stress-Strain Behavior: Measurement, Modeling and Analysis, Springer Netherlands, 2007, pp. 225-234.
[7] E. Andò, S. Hall, G. Viggiani, J. Desrues, P. Bésuelle, Grain-scale experimental investigation of localised deformation in sand: a discrete particle tracking approach, Acta Geotech, 7 (2012) 1-13.
[8] A. Hasan, K. Alshibli, Three dimensional fabric evolution of sheared sand, Granular Matter, 14 (2012) 469-482.
[9] L. Margulies, T. Lorentzen, H.F. Poulsen, T. Leffers, Strain tensor development in a single grain in the bulk of a polycrystal under loading, Acta Mater, 50 (2002) 1771-1779.
[10] U. Lienert, T.S. Han, J. Almer, P.R. Dawson, T. Leffers, L. Margulies, S.F. Nielsen, H.F. Poulsen, S. Schmidt, Investigating the effect of grain interaction during plastic deformation of copper, Acta Mater, 52 (2004) 4461-4467.
[11] J. Oddershede, S. Schmidt, H.F. Poulsen, H.O. Sorensen, J. Wright, W. Reimers, Determining grain resolved stresses in polycrystalline materials using three-dimensional X-ray diffraction, Journal of Applied Crystallography, 43 (2010) 539-549.
[12] R.V. Martins, L. Margulies, S. Schmidt, H.F. Poulsen, T. Leffers, Simultaneous measurement of the strain tensor of 10 individual grains embedded in an Al tensile sample, Mat Sci Eng a-Struct, 387 (2004) 84-88.
[13] E.M. Lauridsen, H.F. Poulsen, S.F. Nielsen, D. Juul Jensen, Recrystallization kinetics of individual bulk grains in 90% cold-rolled aluminium, Acta Mater, 51 (2003) 4423-4435.
[14] S.O. Poulsen, E.M. Lauridsen, A. Lyckegaard, J. Oddershede, C. Gundlach, C. Curfs, D. Juul Jensen, In situ measurements of growth rates and grain-averaged activation energies of

individual grains during recrystallization of 50% cold-rolled aluminium, Scripta Materialia, 64 (2011) 1003-1006.
[15] S.E. Offerman, N.H. van Dijk, J. Sietsma, S. Grigull, E.M. Lauridsen, L. Margulies, H.F. Poulsen, M.T. Rekveldt, S. van der Zwaag, Grain Nucleation and Growth During Phase Transformations, Science, 298 (2002) 1003-1005.
[16] H.F. Poulsen, L. Margulies, S. Schmidt, G. Winther, Lattice rotations of individual bulk grains: Part I: 3D X-ray characterization, Acta Mater, 51 (2003) 3821-3830.
[17] D.J. Jensen, S.E. Offerman, J. Sietsma, 3DXRD characterization and modeling of solid-state transformation processes, Mrs Bull, 33 (2008) 621-629.
[18] H.F. Poulsen, Three-dimensional X-ray diffraction microscopy: mapping polycrystals and their dynamics, Springer2004.
[19] S. Hall, J. Wright, T. Pirling, E. Andò, D. Hughes, G. Viggiani, Can intergranular force transmission be identified in sand?, Granular Matter, 13 (2011) 251-254.
[20] M.L. Rivers, S.R. Sutton, P.J. Eng, Geoscience applications of x-ray computed microtomography, Proceedings of SPIE: Developments in X-Ray Tomography II, 3772 (1999) 78-86.
[21] M.L. Rivers, Y. Wang, T. Uchida, Microtomography at GeoSoilEnviroCARS, Proceedings of SPIE: Developments in X-Ray Tomography IV, 5535 (2004) 783-791.
[22] P. Kenesei, DIGIgrain, http://sourceforge.net/apps/trac/digigrain/wiki, (2012).
[23] J. Wright, *ImageD11*, http://sourceforge.net/apps/trac/fable/wiki/imaged11, (2005).
[24] S. Schmidt, GrainSpotter v. 0.82. , http://fable.svn.sourceforge.net/svnroot/fable/GrainSpotter, (2010).
[25] K. Alshibli, M.B. Cil, P. Kenesei, U. Lienert, Strain tensor determination of compressed individual silica sand particles using high-energy synchrotron diffraction, Granular Matter, in press, (2013).
[26] P. Heyliger, H. Ledbetter, S. Kim, Elastic constants of natural quartz, J Acoust Soc Am, 114 (2003) 644-650.

LIST OF FIGURES

Figure 1

Click here to download high resolution image

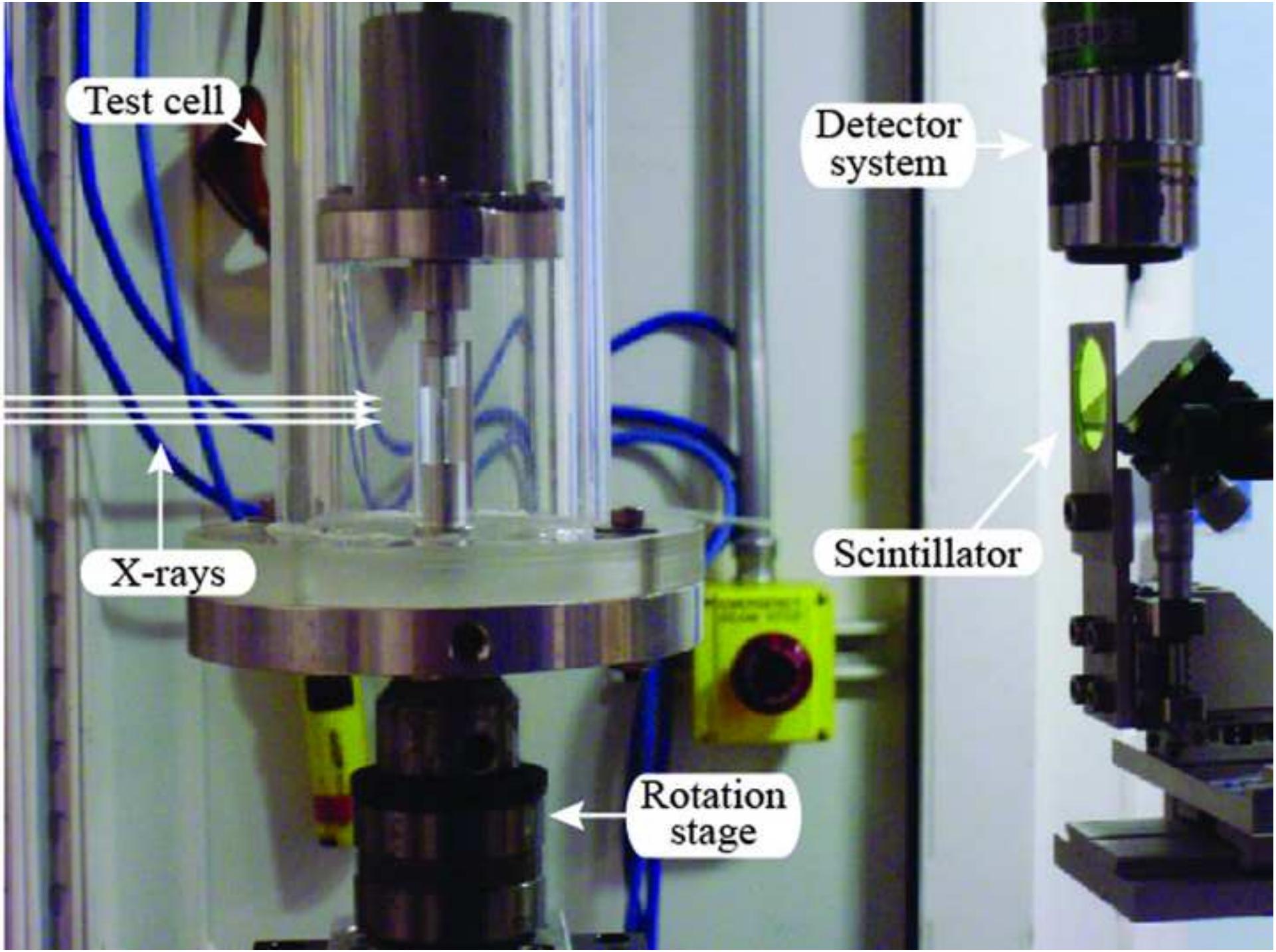

Figure 2

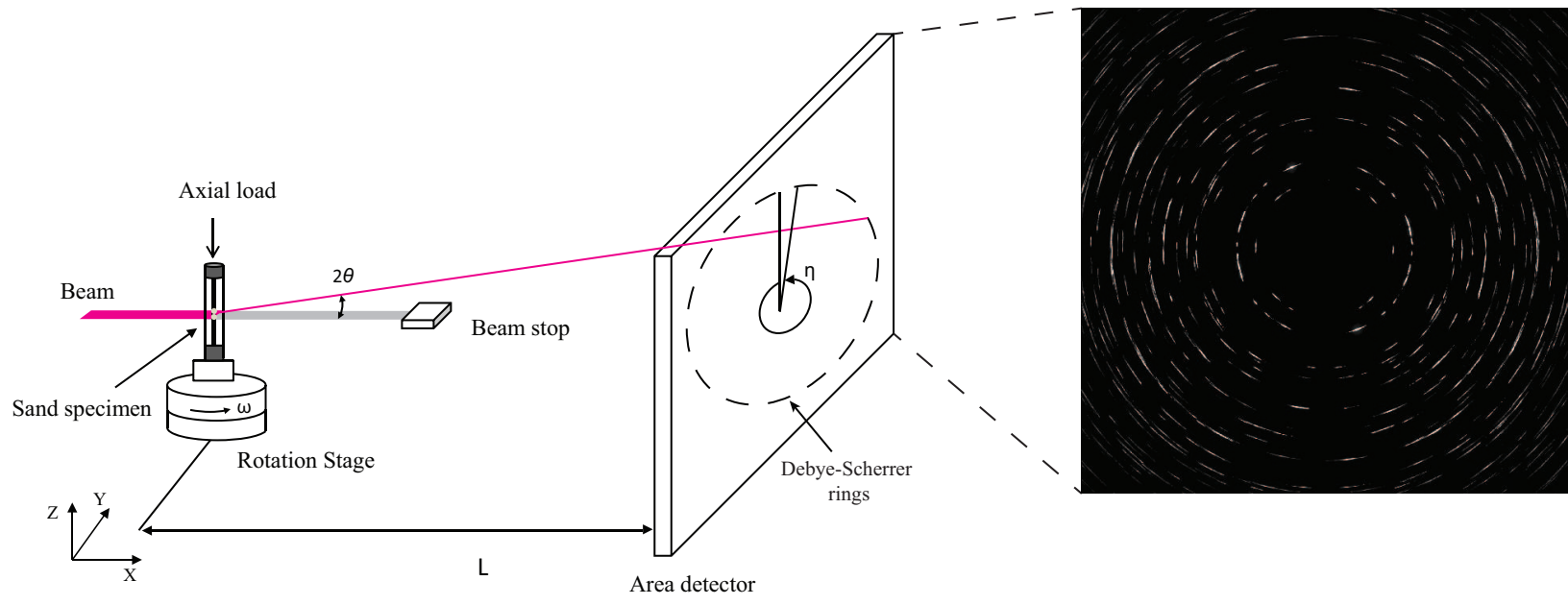
Axial load
Beam
2θ
Beam stop
Sand specimen
ω
Rotation Stage
Z
Y
X
L
Area detector
η
Debye-Scherrer
rings

Figure 3

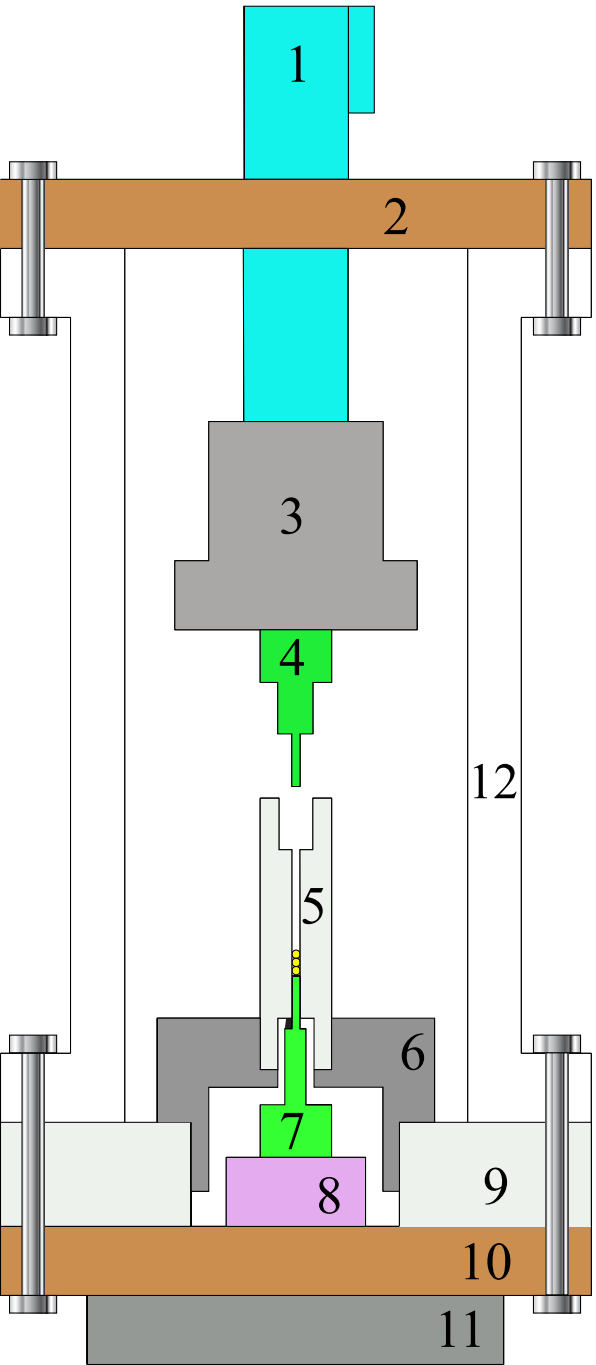

1: Stepper motor to apply axial loading
2: Top cell plate
3: Top load cell
4: Top loading plate
5: Acrylic mold with sand particles
6: Aluminum spacer
7: Bottom loading plate
8: Bottom load cell
9: Acrylic spacer
10: Bottom cell plate
11: Cell-stage connection plate
12: Acrylic chamber

Figure 4

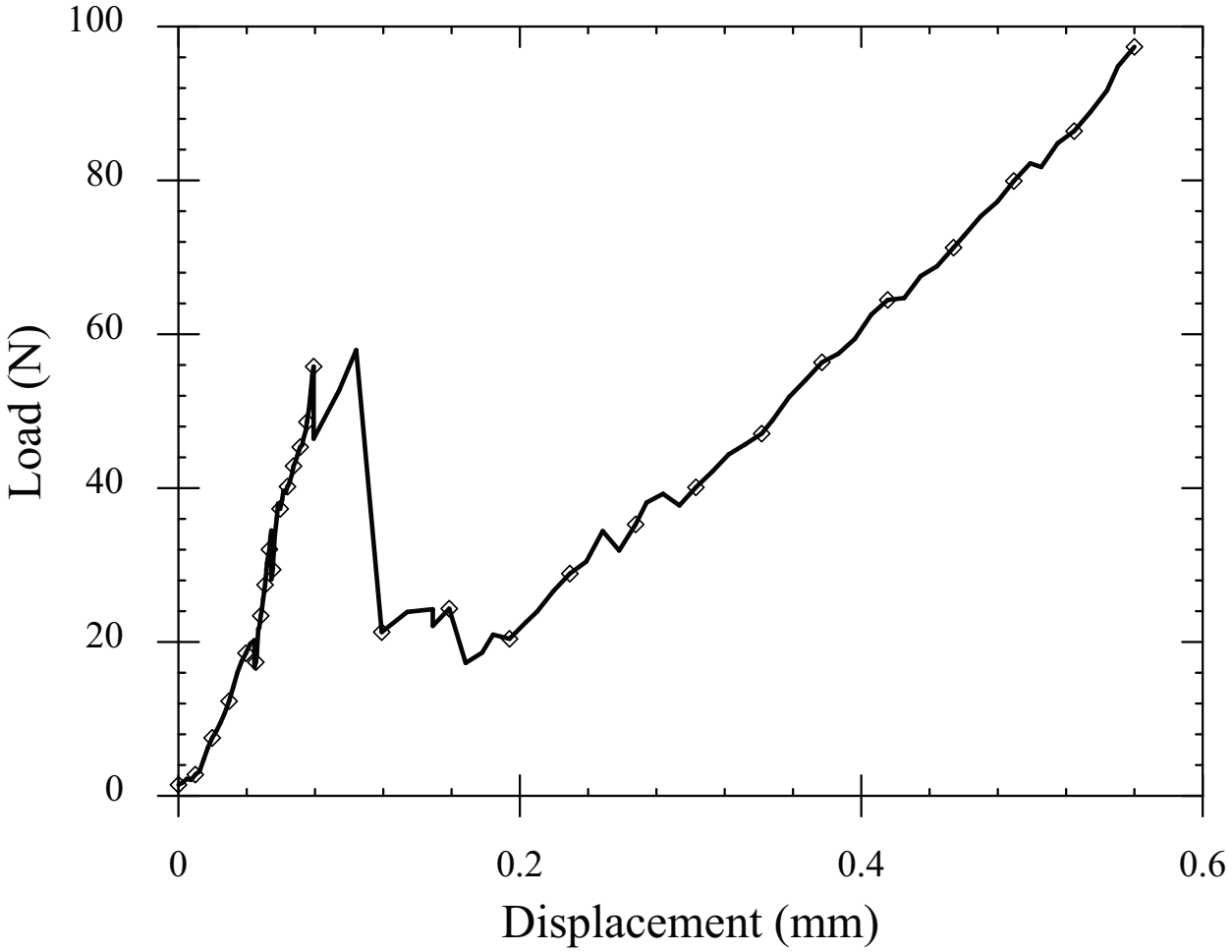

(a)

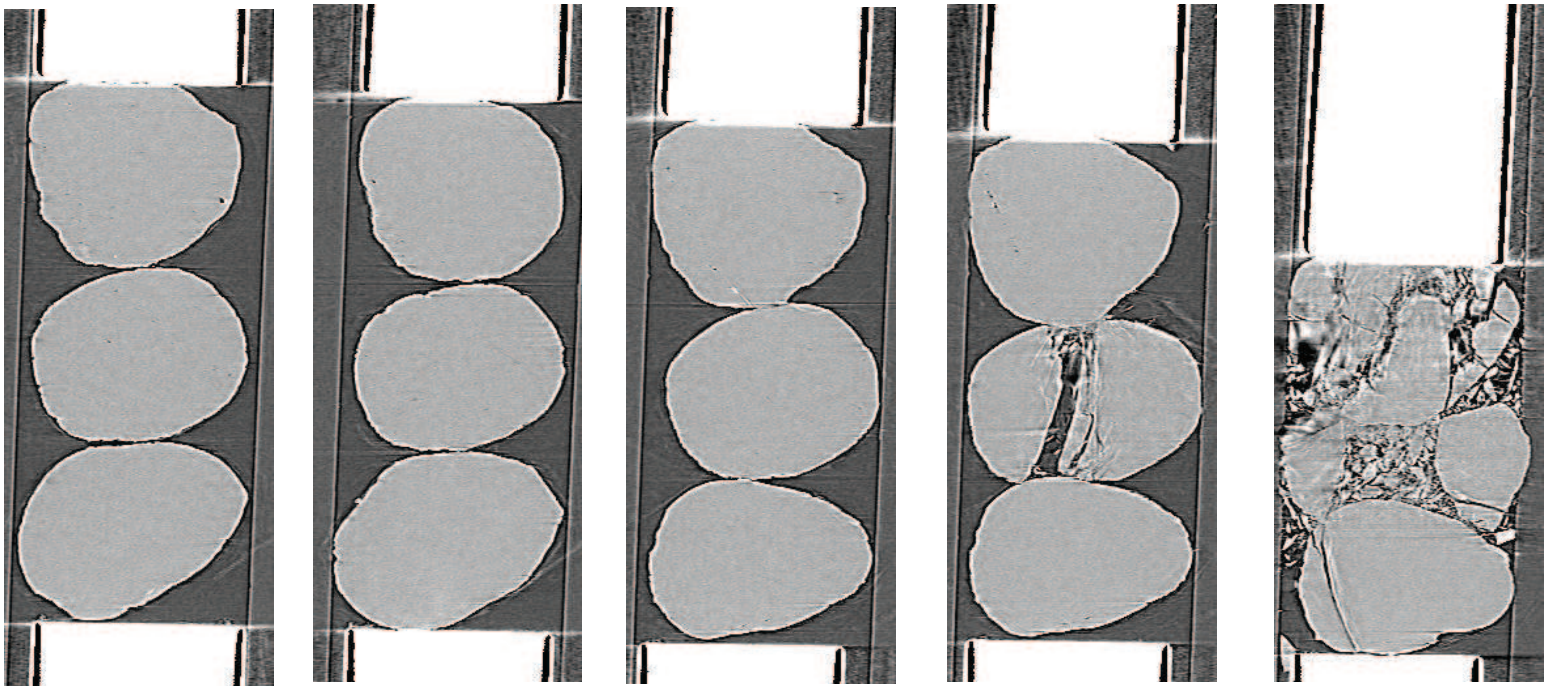

Δ_Z = 0 μm
Load = 0 N

Δ_Z = 54.5 μm
Load = 30 N

Δ_Z = 79.2 μm
Load = 48 N

Δ_Z = 148.5 μm
Load = 22 N

Δ_Z = 560 μm
Load = 88 N

(b)

Figure 5

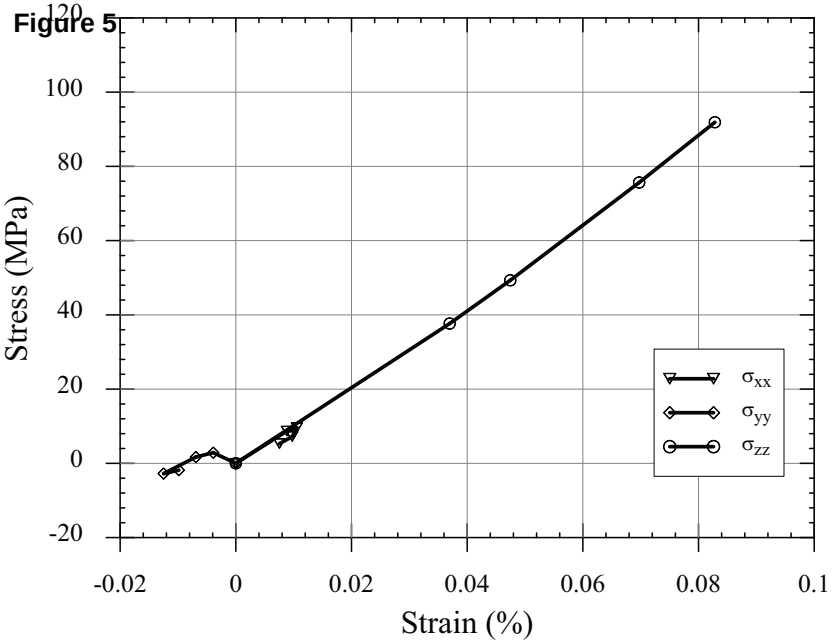
Stress (MPa)
Strain (%)
σxx
σyy
σzz

(a)

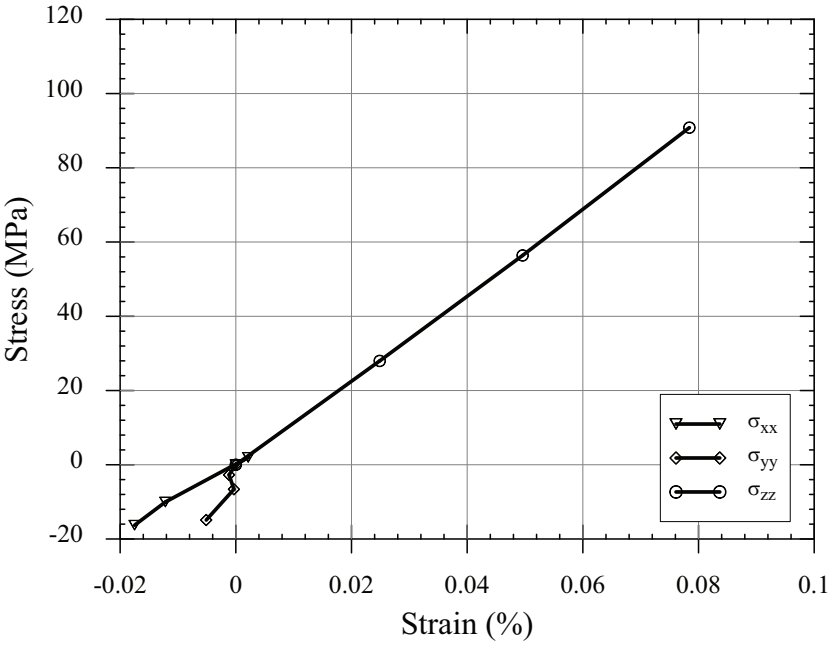
Stress (MPa)
Strain (%)
σxx
σyy
σzz

(b)

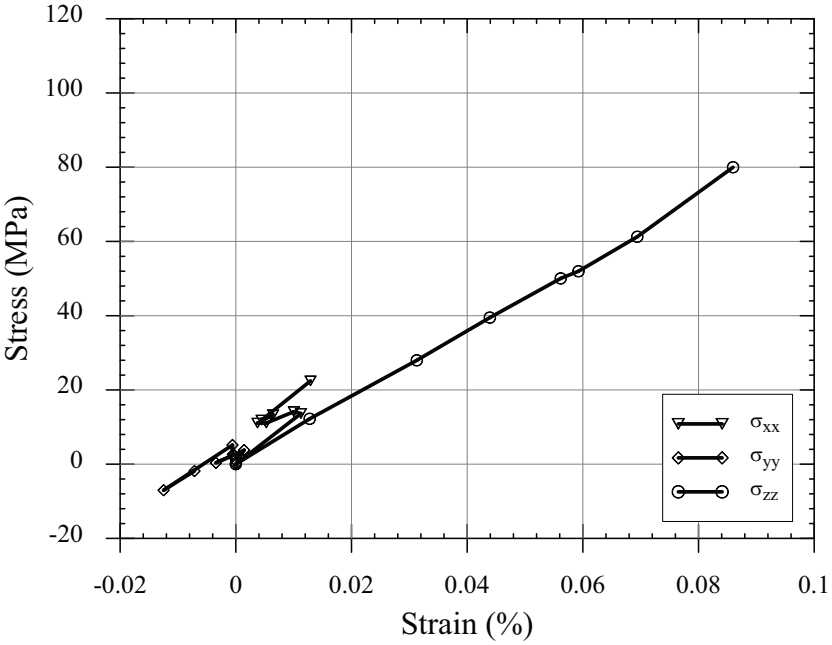
Stress (MPa)
Strain (%)
σxx
σyy
σzz

(c)

Figure 6

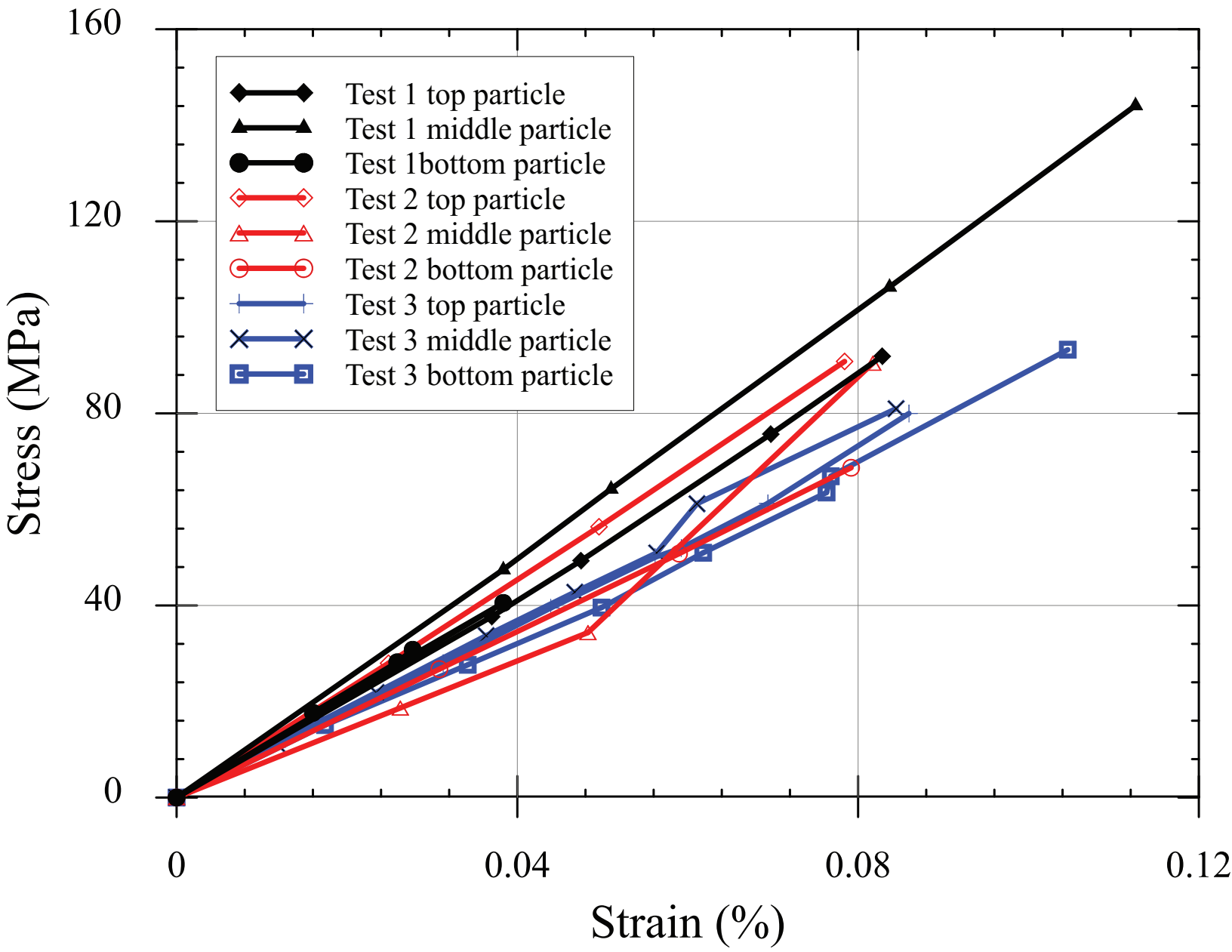
160
120
80
40
0
Stress (MPa)
0
0.04
0.08
0.12
Strain (%)
Test 1 top particle
Test 1 middle particle
Test 1bottom particle
Test 2 top particle
Test 2 middle particle
Test 2 bottom particle
Test 3 top particle
Test 3 middle particle
Test 3 bottom particle